**ORIGINAL PAPER**

# Electrochemical immunosensor nanoarchitectonics with the Ag-rGO nanocomposites for the detection of receptor-binding domain of SARS-CoV-2 spike protein

Aiping Wang[2,3,4] · Yuya Li[2,4] · Xiaojuan You[2,4] · Shoutao Zhang[2,4] · Jingming Zhou[2,4] · Hongliang Liu[2,4] · Peiyang Ding[2,4] · Yumei Chen[2,4] · Yanhua Qi[2,4] · Yankai Liu[2,4] · Chao Liang[2,4] · Xifang Zhu[2,4] · Ying Zhang[2,4] · Enping Liu[2,4] · Gaiping Zhang[1,2,3,4]

## Abstract

As the severe acute respiratory syndrome coronavirus 2 (SARS-CoV-2) poses a grave threat to human life and health, it is essential to develop an efficient and sensitive detection method to identify infected individuals. This study described an electrode platform immunosensor to detect SARS-CoV-2-specific spike receptor-binding domain (RBD) protein based on a bare gold electrode modified with Ag-rGO nanocomposites and the biotin-streptavidin interaction system. The Ag-rGO nanocomposites was obtained by chemical synthesis and characterized by electrochemistry and scanning electron microscope (SEM). Cyclic voltammetry (CV) and electrochemical impedance spectroscopy (EIS) were used to record the electrochemical signals in the electrode modification. The differential pulse voltammetry (DPV) results showed that the limit of detection (LOD) of the immunosensor was 7.2 fg mL$^{-1}$ and the linear dynamic detection range was $0.015 \sim 158.5$ pg mL$^{-1}$. Furthermore, this sensitive immunosensor accurately detected RBD in artificial saliva with favorable stability, specificity, and reproducibility, indicating that it has the potential to be used as a practical method for the detection of SARS-CoV-2.

**Keywords** Electrochemical immunosensor · Ag-rGO nanocomposites · Biotin-streptavidin system · SARS-CoV-2 · Receptor-binding domain

## Introduction

Since the end of 2019, coronavirus disease 2019 (COVID-19), an infectious disease caused by SARS-CoV-2, rapidly swept the world, seriously affecting the normal running of work and life and endangering human health. Although many COVID-19 vaccines have been approved for marketing [1], this is not enough to fully safeguard the health of the population. It is essential to take measures, such as enhancing case detection and contacting tracing to stop the further spread of the virus [2]. Rapid detection technology is another important technology in addition to interception measures such as vaccines. Accurate, simple, cheap, and rapid detection methods can help people find cases early. Therefore, providing accurate and efficient testing methods is necessary for pandemic prevention and control.

There are some measures to detect the SARS-CoV-2: the use of quantitative reverse transcription polymerase chain reaction (RT-PCR) for nucleic acid detection [3], and the use of immune response between antigens and antibodies for serological detection. RT-PCR is undoubtedly the gold standard technique utilized. However, the detection procedure is complex and it has high requirements for professional researchers and experimental equipment [4]. What is more serious is that the RT-PCR has a high false-negative rate [5]; for example, virus nucleic acids were undetectable in a significant number of cases with clinical features of COVID-19 [6], which complicated the prevention and control of the

✉ Gaiping Zhang
zhanggaip@126.com

1 School of Advanced Agricultural Sciences, Peking University, Beijing 100871, China

2 School of Life Sciences, Zhengzhou University, Zhengzhou 450001, Henan, China

3 Longhu Laboratory of Advanced Immunology, Zhengzhou, Henan, China

4 College of Animal Science and Veterinary Medicine, Henan Agricultural University, Zhengzhou 450002, Henan, China

pandemic. Common immunological tests are lateral flow immune assays (LFIA) and electrochemical immunosensors. In the two methods mentioned above, LFIA operation is relatively simple [7]. However, due to its shortcoming in quantitative detection, it is more suitable as an auxiliary diagnostic tool compared to other tests. In contrast, the electrochemical immunosensor based on antigen–antibody response can accurately detect the low concentration of antigen in a short time, which has not only a wide detection range but also a low detection limit [8].

In these 3 years, electrochemical immunosensors have been increasingly used in the detection of SARS-CoV-2. Shimaa Eissa [9] demonstrated a type of electrochemical immunosensor of swabs without transferring or pretreatment of samples. This method effectively improved safety and convenience and the sensitivity of this method can reach 10 pg mL$^{-1}$. Elif Burcu Aydın [10] prepared a sensitive sandwich immunosensor for detection of RBD, which can be reused, and the minimum detection limit can reach 0.577 fg mL$^{-1}$. In the construction of the electrochemical immunosensor, the selection of the target is one of the favorable factors to increase the sensitivity and specificity of the immunosensor. SARS-CoV-2 is a highly diverse envelope-positive single-stranded RNA virus belonging to the coronavirus family [11, 12]. It has four main structural antigens: nucleocapsid (N), spike (S), matrix (M), and envelope (E) [13]. Among them, the S protein is divided into two functionally distinct parts S1 and S2 [14], and the RBD in the S1 can specifically bind to the host cell receptor: angiotensin-converting enzyme 2 (ACE2) [15, 16]. Therefore, screening of RBD as a target for SARS-CoV-2 detection is a priority.

In addition, the electrode material is also an important part for the construction of immunosensor, since it has great biocompatibility [17] and can achieve signal amplification [18]. Graphene is a nanomaterial in which sp$^2$ hybridized carbon atoms are tightly stacked into a single-layer, two-dimensional honeycomb-like lattice structure, with unique lamellar structure [19]. Functionalizing graphene such as reduced graphene oxide (rGO) is widely used in the material field because of its large specific surface area and good electrical conductivity as well as thermal stability [20]. In this study, rGO was introduced as the electrode nanomaterial. However, rGO tends to form flaky agglomerates in water, thus hindering electron transport. Therefore, silver nanoparticles were introduced into the rGO for amplifying signals, enhancing biocompatibility [21], reducing the accumulation of graphene sheets, and facilitating electron transfer [22, 23]. Furthermore, compared with the precious nanometals such as Au [24], Pd [25], and Pt [26], the introduction of silver nanoparticles can effectively reduce the difficulty and cost of preparation. At the same time, nafion was used as a dispersant to overcome aggregation. Eventually, we developed Ag-rGO nanocomposites as the electrode material to achieve the signal amplification.

What's more, studies have shown that the accession of biotin-streptavidin system is an efficient way to immobilize more biotin-modified capture probes [27] and improve LOD and selectivity [28]. The advantage of this system is that one molecule of SA can provide four biotin-binding sites [27, 29]. Therefore, in this study, the biotin was conjugated to the anti-RBD monoclonal antibody at first. Then, the biotin-streptavidin system was utilized as the bridge to link the Ag-rGO nanocomposites and RBD antibody in this immunosensor.

Given the evolution of today's global pandemic, there is an urgent need for faster and more sensitive methods to detect this rapidly spreading deadly disease to achieve fast control and diagnosis of confirmed cases of the virus and close contracts. In this study, an efficient and accurate biosensor was made by Ag-rGO nanocomposites and biotin-streptavidin system for RBD detection.

## Materials and methods

### Chemicals

SARS-CoV-2 RBD antibody, SARS-CoV-2 RBD (His Tag), and pseudotyped virus were prepared in the molecular immunology laboratory, Zhengzhou University. Biotin labeling kit was acquired from Elabscience Biotechnology Co., Ltd. (Wuhan, China). SA and artificial saliva were obtained from Beijing Solarbio Science & Technology Co., Ltd (Beijing, China). GO was provided by XFNANO Materials Tech. Co., Ltd (Nanjing, China). Nafion (Nf) and BSA were purchased from Sigma Chemicals (St Louis, USA). AgNO$_3$ was brought from Sinopharm Chemical Reagent Co., Ltd (Shanghai, China). NaBH$_4$ was acquired from Shanghai Macklin Biochemical Co., Ltd (Shanghai, China). Phosphate buffer solution (PBS, pH 7.4) was prepared from 0.1 M Na$_2$HPO$_4$, 0.1 M KH$_2$PO$_4$, and 0.1 M KCl, which was used as an electrolyte in the electrochemistry measurements.

### Apparatus

All electrochemistry measurements were performed with the CHI 660E electrochemical workstation (Shanghai Chenhua Instrument Co., Ltd., Shanghai, China). The electrochemical workstation consists of the working electrode (gold electrode), the counter electrode (platinum electrode), and the reference electrode (saturated calomel electrode, SCE) (Gaoss Union Co., Ltd, Wuhan, China). Thermo Nanodrop 2000c spectrophotometer (Thermo Fisher Scientific Co., Ltd., USA), scanning electron microscope (Zeiss Gemini

300), and X-ray diffractometer (X'Pert PRO, Netherland) were used to characterize the nanomaterials. Ultrapure water in all experiments was obtained by Barnstead Nanopure ultrapure water meter. SB25-12DTD ultrasonic cleaning machine (Scientz Co., Ltd., Ningbo, China) was used for material dispersion and related cleaning.

## Preparation of Ag-rGO nanocomposites

The preparation process of Ag-rGO is shown in Fig. 1A with reference to previous studies [20]. Fifty milligrams of GO was dispersed with 30 mL of ethylene glycol and stirred at high speed for 1 h. After that, 200 mg of $AgNO_3$ was added in 15 mL of ethylene glycol with 5 mL of ultrapure water. Then, the $AgNO_3$ dispersion was slowly added to the GO dispersion, and stirred at 50℃ for 2 h. After a full reaction, 20 mL of $NaBH_4$ (0.1 mol $mL^{-1}$) was added drop by drop and the mixture was stirred at 110℃ for 2 h. After that, the solution was centrifuged at 6124×g for 10 min, and the collected precipitation was washed with ultrapure water and dried in an oven at 80℃. Finally, the material was ground into powder and stored at 4℃. Before experiment, 3 mL of the mixture consisting of ultrapure water and 0.4%Nafion (Nf) in a ratio of 3:1 was added to 0.9 mg Ag-rGO powder. The uniform Ag-rGO-Nf solution (0.3 mg $mL^{-1}$) was obtained under sonicated treatment for 2 h.

## Preparation of biotin-anti-RBD antibody

Anti-RBD antibody was labeled with biotin following the kit instructions and the diagram is shown in Fig. 1B. The antibody was mixed with $NH_2$-Reactive Biotin at a ratio of 1:20 molecular weight, incubated for 30 min protected from light, and then collected by centrifugation to obtain the biotinylated monoclonal antibody.
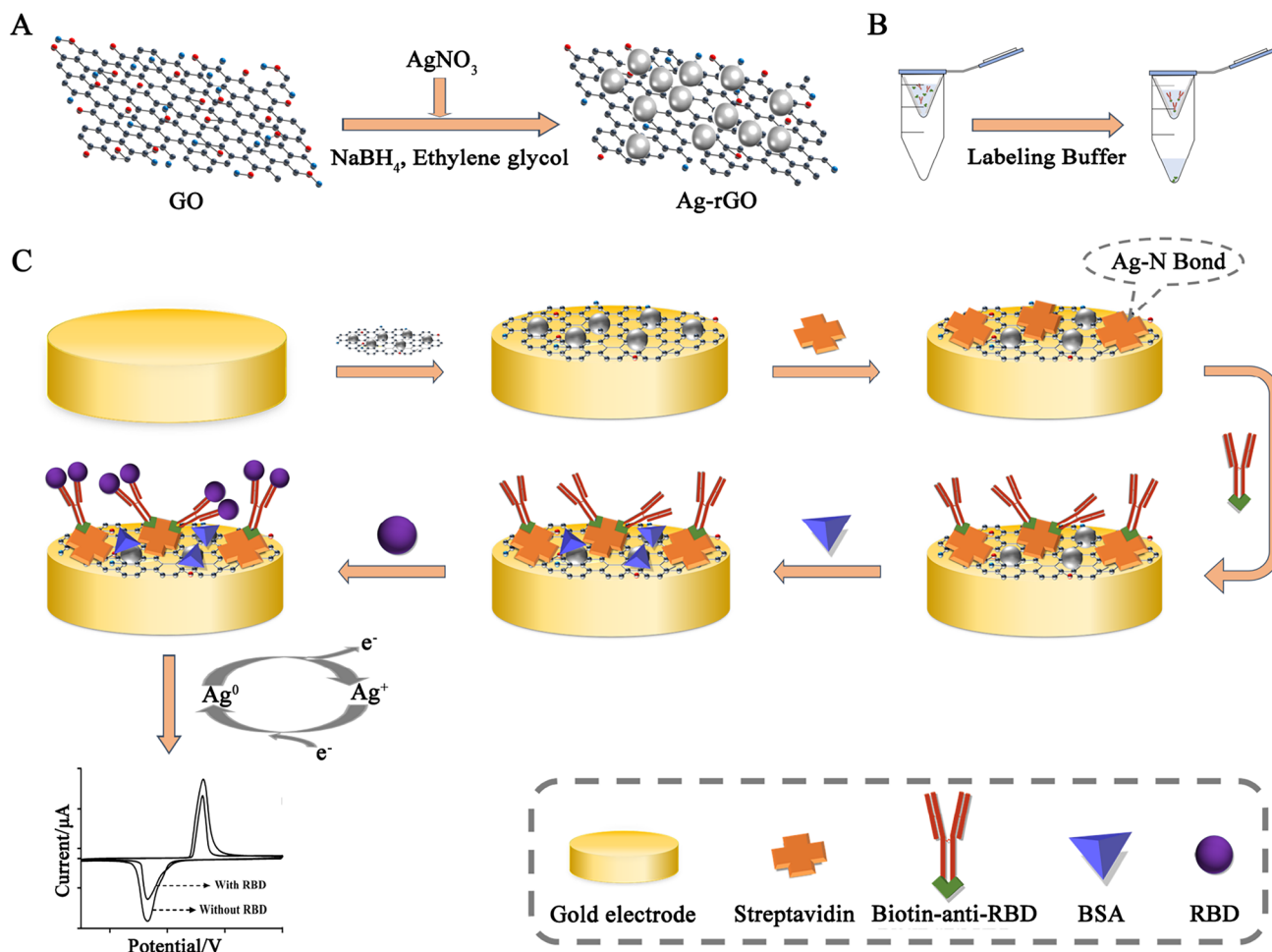


Fig. 1 Schematic illustrations of the preparation of Ag-rGO (**A**). The preparation of biotin-anti-RBD antibody (**B**). The preparation of electrochemical immunosensor (**C**)

## Preparation of electrochemical immunosensor

Before preparing the sensors, the gold electrode was polished with a powder of 0.3 μm and 0.05 μm. After that, the electrode was washed with anhydrous ethanol and ultrapure water respectively, and then dried with nitrogen. Figure 1C shows the construction process of the electrochemical immunosensor. First, the 10 μL of Ag-rGO-Nf nanocomposites was dropped on the surface of the gold electrode. After drying at room temperature, the 20 μL SA and biotin-anti-RBD antibody were dropped respectively to immobilize the antibody. During this process, the biotin-anti-RBD was linked to the modified electrode through streptavidin–biotin interactions [30]. Eventually, the remaining active sites were blocked with 10 mL 0.1%(w/t) BSA. During the immunosensor construction, all incubations were performed at 37℃ and each incubation was followed by a rinse with ultrapure water.

## Electrochemical measurement

The construction process of the immunosensor was characterized by CV and EIS. The CV measurements were made in the range of $-0.3 \sim 0.5$ V at the scanning rate of 50 mV s$^{-1}$ in 0.1 M PBS (0.1 M, pH 7.4) to characterize immunosensor development. The EIS measurements were performed in the PBS solution containing 5 mM $[Fe(CN)_6]^{3-/4-}$ with an initial potential of 0.226 V, an amplitude of 0.005 V, and a frequency range of $0.1 \sim 10^5$ Hz. Moreover, the response performance of the immunosensor was measured in PBS solution (0.1 M, pH 7.4) by DPV with a voltage range of $-0.05 \sim 0.15$ V, an amplitude of 0.05 V, a pulse width of 0.05 s, a sampling width of 0.0167, and a pulse period of 0.5 s. Different concentrations of RBD were added to the modified electrode for measurement, and the antigen–antibody immune complex formed after the antigen bind to antibody hindered electron transfer, thereby reducing the electrochemical signal. This allows us to track changes in the current signal for sensor performance analysis.

## Preparation of simulated samples

Simulated samples were prepared by mixing commercialized artificial saliva and the SARS-CoV-2 spike protein pseudotyped virus. The simulated sample was diluted by artificial saliva to the concentration of $0.315 \sim 315$ TCID$_{50}$/mL.

## Result and discussion

### Characterization of Ag-rGO nanocomposites

In the preparation process of Ag-rGO nanocomposites, the oxygen functional groups of GO promoted the initial attachment of free Ag$^+$ in solution through electrostatic interactions. Afterwards, Ag$^+$ was reduced to silver nanoparticles in the presence of ethylene glycol and NaBH$_4$ and attached to GO. In this process, GO provides the attachment area for the silver nanoparticles and the formation of AgNPs also avoids the lamellar stacking of GO. The Ag-rGO nanocomposite formed when GO was reduced to rGO by the strong reducing agent. Following the successful preparation of the material, its structure and morphology were characterized by XRD and SEM respectively.

The UV–Visible spectra of GO are shown in Fig. 2A, where GO showed absorption peaks at around 230 nm and 300 nm, which was probably due to the $\pi \rightarrow \pi^*$ transition of the C–C bond and the $n \rightarrow \pi^*$ transition of the C=O bond. After the reduction of GO by NaBH$_4$, the peak was red-shifted to around 260 nm, which indicated that the electronic conjugation within the graphene sheet was restored [31] and GO was reduced to rGO. Furthermore, the characteristic peak of AgNPs appeared at 410 nm [23], suggesting that the AgNPs were successfully formed on the rGO. The X-ray diffraction (XRD) patterns of GO and Ag-rGO are exhibited in Fig. 2B. The GO showed a characteristic diffraction peak at 10.95 [32], which is caused by the oxygen functional groups in GO. The Ag-rGO demonstrated four diffraction peaks at $2\theta = 38.09°$, $44.20°$, $64.39°$, and $77.42°$, which could be corresponded to Ag (111), Ag (200), Ag (220), and Ag (311) on the central cubic (fcc) crystal [33]. In contrast to the spectra of GO, the disappearance of GO diffraction peaks in the synthetic composites indicates the presence of rGO exfoliation [20].

Eventually, the morphology of the nanocomposites was characterized using SEM. GO showed an obvious folded lamellar state in Fig. 2C, and these corrugated sheets were due to the disruption of the planar sp$^2$ carbon sheets by the introduction of sp$^3$-hybridized carbon during oxidation [34]. The morphology of Ag-rGO is shown in Fig. 2D; the rGO had a large and compact surface, showing curved and folded sheets, and was uniformly covered with AgNPs, indicating that AgNPs were successfully reduced to the surface of rGO. The above results demonstrated that the preparation of Ag-rGO was successful.

### Electrochemical behavior of the immunosensor

CV was used to confirm each modification of the electrode. As shown in Fig. 3A, the bare gold electrode (curve a) had no redox peak at a given voltage due to the lack of electroactive substances. After Ag-rGO-Nf modification (curve b), it showed obvious redox current response, which was due to AgNPs possessing great ability to gain or lose electrons [35], indicating that it can act as a redox probe for electron transfer with the electrode surface. When SA (curve c) was added to the electrode surface, it can be fixed on the modified electrode by Ag–N bond [36], while the decrease in current
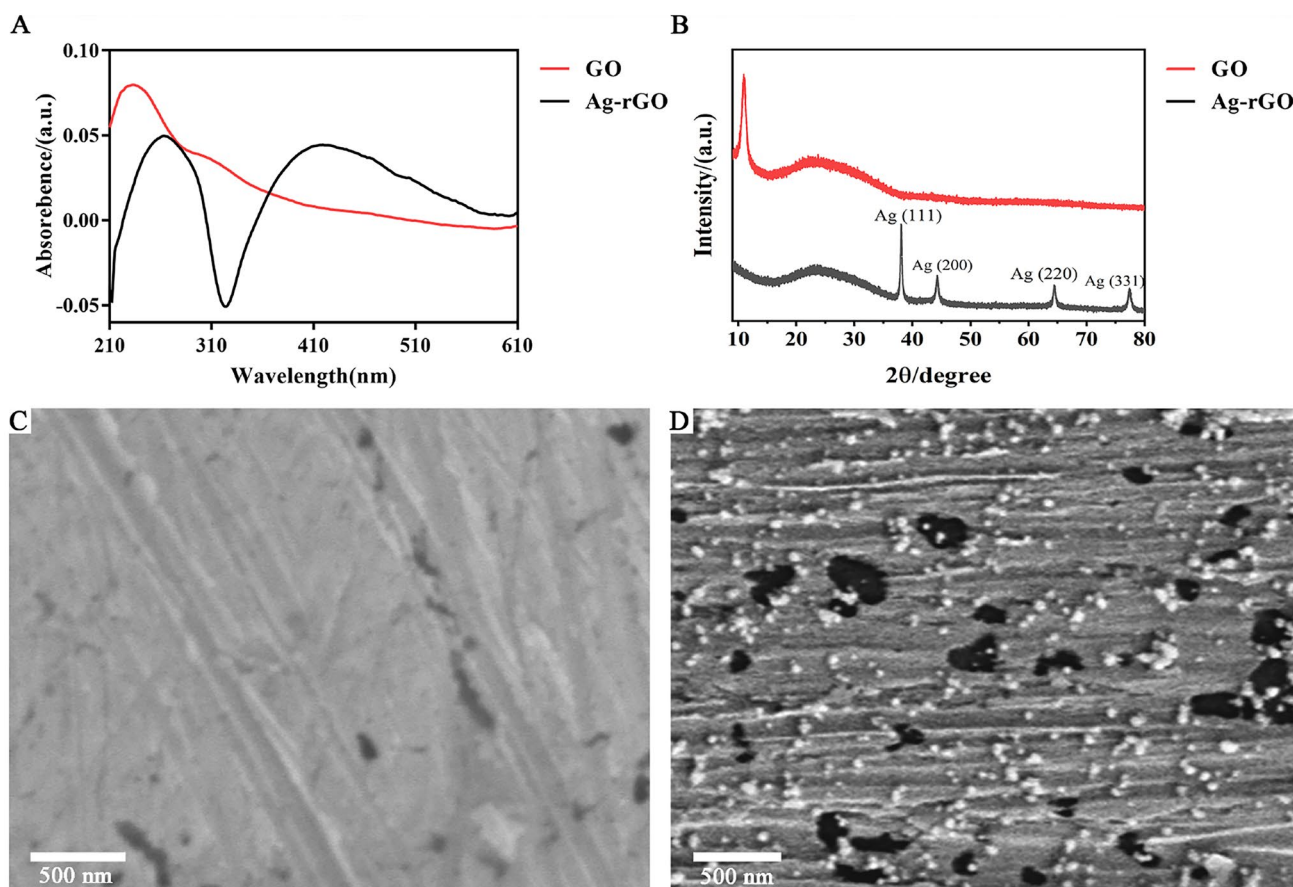
**Fig. 2** The UV–vis spectra (**A**) and XRD pattern (**B**) of GO and Ag-rGO; SEM images of GO (**C**) and Ag-rGO (**D**)

indicated that SA as an insulating biomolecule impeded electron transfer. After immobilization of biotin-anti-RBD antibody (curve d), the redox peak was decreased owing to the bioactive material possessing the ability of impeding electron transfer [30]. With the addition of BSA (curve e), the non-specific binding site was blocked and the electron

transfer rate was reduced, leading to a further decrease in current signal intensity. After the addition of RBD (curve f), the current intensity reached a minimum due to the formation of immune complexes.

EIS was also used for electrochemical characterization of each step of the electrode modification. The Nyquist
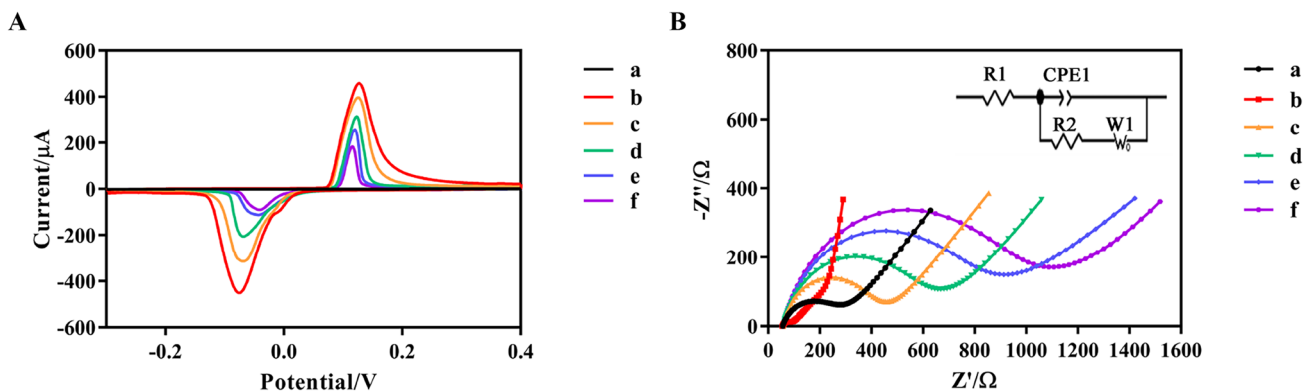


**Fig. 3** CVs (**A**) and EIS (**B**) of the same electrode at different stages. (a) bare gold electrode, (b) Ag-rGO-Nf/gold electrode, (c) SA/Ag-rGO-Nf/gold electrode, (d) biotin-anti-RBD antibody/SA/Ag-rGO-Nf/gold electrode, (e) BSA/biotin-anti-RBD antibody/SA/Ag-rGO-Nf/gold electrode, and (f) RBD/BSA/biotin-anti-RBD antibody/SA/Ag-rGO-Nf/gold electrode
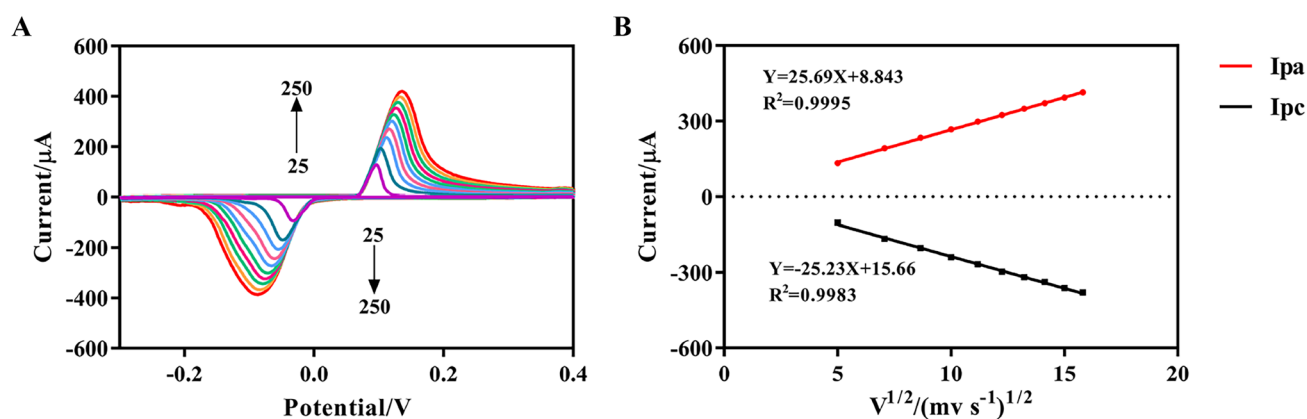
**Fig. 4** (**A**) CVs of the electrochemical immunosensor at the different scan rates: 25, 50, 75, 100, 125, 150, 175, 200, 225, 250 mV s$^{-1}$. (**B**) The relationship between the square root of the sweep rate and the redox peak current

representation contains a linear portion at low frequencies and a semicircle portion at high frequencies. The semicircle portion is related to the electrochemical process subject to electron transfer. And the diameter of the semicircle represents the electrode transfer resistance ($R_{ct}$), the larger the diameter, the larger the $R_{ct}$. As shown in Fig. 3B, the gold electrode (curve a) had a small $R_{ct}$, and the $R_{ct}$ decreased after the incubation of Ag-rGO-Nf nanocomposites (curve b), which meant that the nanomaterial had better electrochemical activity and could enhance the electron transfer rate. With the addition of bioactive substances such as SA (curve c), biotin-anti-RBD antibody (curve d), and BSA (curve e), the $R_{ct}$ of the Nyquist plot gradually increased, indicating that the successful immobilization of proteins hindered the electron transfer efficiency [37]. Eventually, $R_{ct}$ reached the maximum after incubation with RBD (curve f), indicating that the immunocomplex formed by biotin-anti-RBD antibody and RBD further impeded electron transport. The results of EIS were consistent with CV, suggesting that the fabrication of electrochemical immunosensor was successful.

In addition, the immunosensor was further electrochemically characterized by CV at different scan rates. As shown in

Fig. 4A, the peak anode peak current (*Ipa*) and the peak cathode current (*Ipc*) of the immunosensor gradually increased with the scan rates ranging from 25 to 250 mV s$^{-1}$. The linear regression equations for *Ipa* and *Ipc* were obtained in Fig. 4B as $Ipa = 25.69v^{1/2} + 8.843$ with a correlation coefficient of 0.9995 and $Ipc = -25.23v^{1/2} + 15.66$ with a correlation coefficient of 0.9983, and the square root of the scan rate ($v^{1/2}$) was linear in the range of 25 ~ 250 mV s$^{-1}$. The results demonstrated that the redox reaction process of the immunosensor was controlled by diffusion [38].

## Optimization of experimental conditions

In order to obtain the best experimental results, some experimental conditions were optimized by CV. Firstly, four concentrations (1, 5, 15, and 25 μg mL$^{-1}$) and four incubation times (40, 60, 80, and 100 min) of SA were set, respectively. As shown in Fig. 5A, the changes in current ($\Delta I$) gradually increased with increasing incubation concentration and time, reached a highest value when 15 μg mL$^{-1}$ of SA was incubated for 80 min, and then remained stable with the increasing of time or concentration. Therefore, to save material and
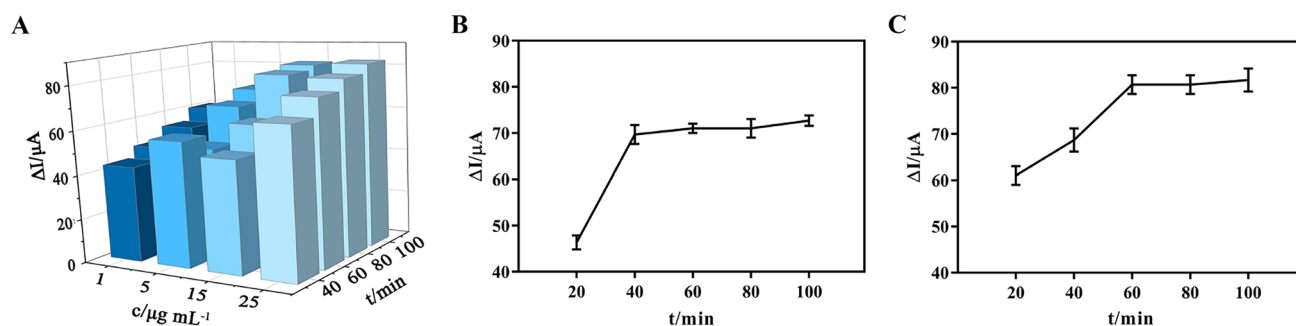


**Fig. 5** Optimization of the incubation concentration and time of SA (**A**). The incubation time of biotin-anti-RBD antibody (**B**). The incubation time of RBD (**C**) (error bar = SD, $n = 3$)

**Fig. 6** (**A**) The DPV current values of the immunosensor at different concentrations (0.015, 0.1, 0.63, 3.98, 25.1, 158.5 pg mL$^{-1}$) of RBD. (**B**) Calibration plot of $\Delta I$ versus the logarithm of RBD concentrations (error bar = SD, $n$ = 3)
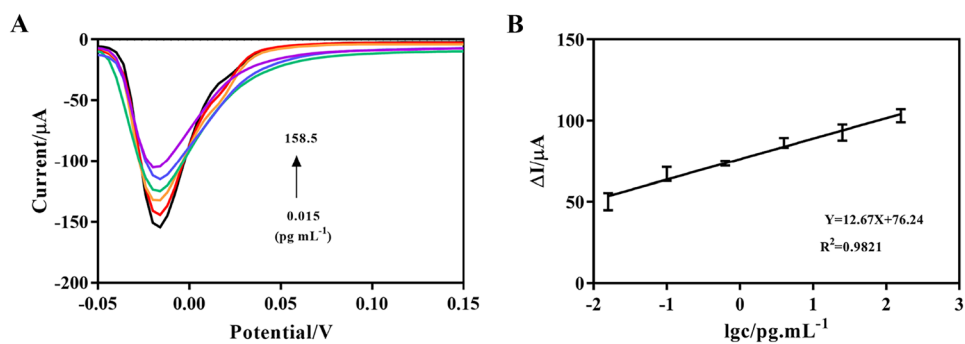
time, the optimal incubation concentration and time were determined to be 15 μg mL$^{-1}$ and 80 min.

In addition, the biotin-anti-RBD antibody incubation time also affected the performance of the immunosensor. As shown in Fig. 5B, the reaction time was investigated ranging from 20 to 100 min. Due to the poor electrical conductivity of the biological active substances, $\Delta I$ gradually increased and reached a maximum at 40 min, then remained stable. Therefore, the optimal incubation time was determined to be 40 min.

Finally, the effect of the RBD reaction time on the performance of the electrochemical sensor was investigated, with reaction time ranging from 20 to 100 min. Figure 5C shows that $\Delta I$ gradually increased with increasing incubation time and reached a maximum at 60 min, followed by a slight decrease. The results indicated that the immunocomplexes formed on the immunosensor surface were saturated. Hence, 60 min was determined as the optimal incubation time for subsequent experiments.

## Analytical performance of the immunosensor

The DPV current values of the immunosensor were measured after incubation with different concentrations of RBD in 0.1 M PBS under optimal conditions. As shown in Fig. 6A, the DPV curve gradually decreased as the RBD concentration increased from 0.015 to 158.5 pg mL$^{-1}$. In addition, the logarithmic calibration plot in Fig. 6B showed that the current response was linearly related to the logarithmic value of the RBD concentration with the linear equation of $Y = 12.67X + 76.24$ ($Y$ represents $\Delta I$ and $X$ represents

the logarithmic value of RBD protein concentration) and a correlation coefficient of 0.9821. The DPV detection results denoted that the linear range of the immunosensor was 0.015 ~ 158.5 pg mL$^{-1}$, and the LOD was calculated as 7.2 fg mL$^{-1}$ (LOD = 3SB/$m$, SB stands for standard deviation without RBD, $m$ stands for slope of calibration curve, $n$ = 10 [39, 40]).

As shown in Table 1, the LOD of this electrochemical immunosensor (7.2 fg mL$^{-1}$) has a significant advantage over the studies by Basca Wadramani (0.7 nM), Birjana Moisoska (260 nM), and Yang Yi (0.2 ng mL$^{-1}$). In addition, compared with the studies of Basca Vadramani (14 ~ 1400 nM) and Arzum Eldem (0.5 ~ 10 ng mL$^{-1}$), the proposed method has a wider linear detection range (0.015 ~ 158.5 pg mL$^{-1}$). The results may be attributed to several factors: (i) The excellent electrical conductivity and high biocompatibility of the Ag-rGO nanocomposite. rGO provides a large specific surface area for the attachment of AgNPs, and the formation of AgNPs enables the material to transfer electrons efficiently. (ii) The introduction of the biotin-streptavidin system enables the streptavidin to act as a sensitive trap and efficiently capture the biotin-labeled monoclonal antibody. (iii) The high affinity and specificity of the antibody for the RBD allow it to sensitively capture the antigen and bind to it to form an immune complex.

## Stability, reproducibility, and specificity of the immunosensor

To characterize the stability of the BSA/biotin-anti-RBD antibody/Ag-rGO immunosensor, one immunosensor was

**Table 1** Comparison of different analytical methods for SARS-CoV-2 detection

| Materials | Detection technology | Linear range | Limit of detection | Refs |
|---|---|---|---|---|
| Cobalt-functionalized TiO2 nanotubes | Amperometric immunoassay | 14 to 1400 nM | ~0.7 nM | [41] |
| Graphene | Square wave voltammetry | - | 260 nM | [42] |
| - | Fluorescence | 2.0–14.6 ng mL$^{-1}$ | 0.2 ng mL$^{-1}$ | [43] |
| - | Amperometric immunoassay | 0.5–10 ng mL$^{-1}$ | 0.19 ng mL$^{-1}$ | [44] |
| Ag-rGO nanocomposites | Differential pulse voltammetry | 0.015 ~ 158.5 pg mL$^{-1}$ | 7.2 fg mL$^{-1}$ | This work |

**Fig. 7** (**A**) The stability of the immunosensor after 20 scanning cycles. (**B**) The stability of the immunosensor at various storage periods. (**C**) The reproducibility of the immunosensor after incubation of 100 pg mL$^{-1}$ of RBD using five identical sensors. (**D**) The selectivity of the immunosensor for 200 pg mL$^{-1}$ HPV protein, 200 pg mL$^{-1}$ VZV protein, 200 pg mL$^{-1}$ SARS-CoV protein, 100 pg mL$^{-1}$ RBD protein, and 100 pg mL$^{-1}$ mixture of above proteins with 100 pg mL$^{-1}$ RBD ($n=3$)
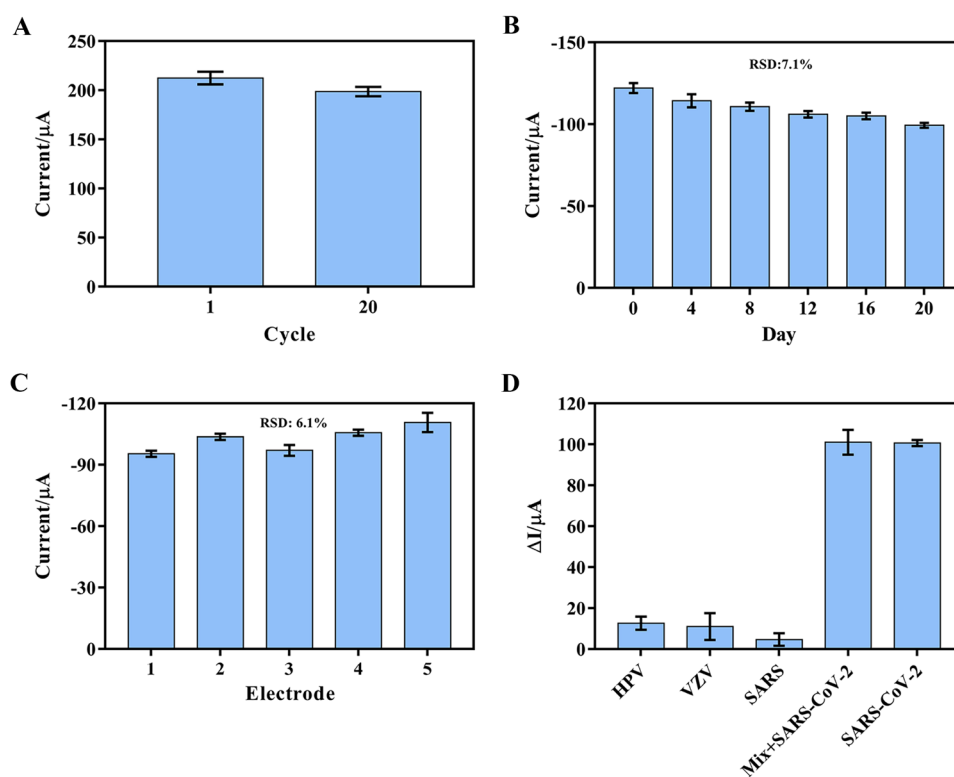


continuously scanned 20 cycles using CV. The result is shown in Fig. 7A, where the current response value of the immunosensor was reduced by 6.4% compared to the initial value. In addition, the same batch of treated immunosensors was placed at 4℃ and tested every 4 days. As shown in Fig. 7B, the current response values of the sensor were 90.71% and 86.07% on day 8 and day 16, respectively, suggesting the good stability of the electrochemical immunosensor in this study.

The reproducibility of an immunosensor is also an important indicator to evaluate the applicability of the immunosensor. The current variation of the immunosensor was tested using five identical sensors. Figure 7C shows that the relative standard deviation (RSD) of the five immunosensors was 6.1%. The result indicated that the immunosensor was reliable.

Specificity is another important feature to demonstrate the suitability of the sensor. To test the cross-reactivity of the sensor, the current responses of HPV, VZV, and SARS-CoV structural proteins incubated on the immunosensor were recorded. The specificity of the sensor was measured by dropping 200 pg mL$^{-1}$ interfering agents, 100 pg mL$^{-1}$ RBD protein, and a mixture of RBD and interfering agents on the same treated immunosensors. As shown in Fig. 7D, the current of the immunosensor was essentially unchanged with the addition of interfering substances only. The change in current with the addition of a mixture of interferent and RBD was essentially the same as with the addition of RBD only, indicating that the immunosensor had good selectivity for RBD and no cross-reactivity caused by HPV, VZV, and SARS-CoV proteins.

## Antigen protein and simulated virus spiked sample analysis

The immunosensor was applied to the measure SARS-CoV-2 RBD protein samples in artificial saliva, and the RBD content was determined by DPV. Artificial saliva samples containing 1 pg mL$^{-1}$, 10 pg mL$^{-1}$, and 100 pg mL$^{-1}$ RBD proteins were measured respectively. As shown in Table 2, the

**Table 2** The results of measurement of RBD protein samples in artificial saliva ($n=3$)

| The added amount of RBD (pg mL$^{-1}$) | RBD found (mean ± standard deviation; pg mL$^{-1}$) | Recovery (mean ± standard deviation; %) | Relative standard deviation (%) |
|---|---|---|---|
| 1 | 0.960 ± 0.087 | 96.00 | 9.08 |
| 10 | 9.871 ± 0.510 | 98.71 | 5.16 |
| 100 | 94.690 ± 8.131 | 94.69 | 8.59 |

**Fig. 8** (**A**) The DPV current value of the immunosensor at different concentrations (315, 31.5, 3.15, 0.315 TCID$_{50}$/mL) of simulated virus incubation. (**B**) The relationship between the different concentrations of simulated virus and the $\Delta I$
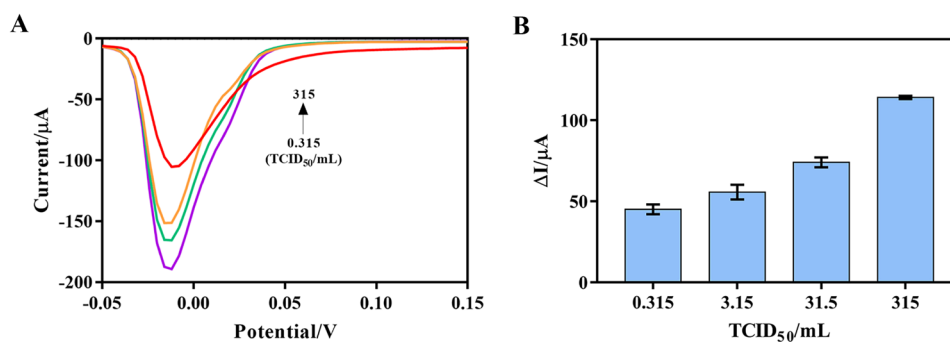


recovery rates were 94.69~98.71%, and the relative standard deviations were 5.16~9.08%, which indicated that the accuracy of the proposed method was acceptable.

To verify the effectiveness of the BSA/biotin-anti-RBD antibody/SA/Ag-rGO-Nf/gold electrode immunosensor, the simulated virus diluted by commercial artificial saliva was incubated on the modified electrode and detected by DPV. The voltammetry in Fig. 8 showed that the current signal decreased after incubation of the simulated virus, and $\Delta I$ increased with the increase of the simulated virus concentration. The result indicated that the immunosensor could successfully detect the RBD on the simulated virus diluted with artificial saliva. Suggested that the immunosensor has the potential to detect viruses in real saliva samples.

## Conclusion

In this study, an efficient and ultrasensitive biosensor was prepared successfully based on BSA/biotin-anti-RBD antibody/SA/Ag-rGO-Nf/gold electrode platform to detect SARS-CoV-2 RBD. The large specific surface area of rGO increased the loading of AgNPs, and the good electrical conductivity of AgNPs promoted electron transfer and signal amplification. The utilization of the biotin-streptavidin system increased the amount capture of RBD, which made this immunosensor sensitive and selective. The results suggested that this biosensor had a linear dynamic range of 0.015 to 158.5 pg mL$^{-1}$ and the LOD was 7.2 fg mL$^{-1}$. As the results from CV and DPV, this immunosensor can detect the RBD in artificial saliva with recovery rates ranging from 94.69 to 98.71% with great reproducibility and stability, which may provide ideas for the quality control of recombinant subunit vaccine by detecting the content of spike protein. Furthermore, the biosensor was capable of successfully detecting the RBD on the simulated viral environment diluted with artificial saliva, suggesting its potential as a practical detection method in the future.

## Declarations

**Conflict of interest** The authors declare no competing interests.

## References

1. Dong Y, Dai T, Wei Y, Zhang L, Zheng M, Zhou F (2020) A systematic review of SARS-CoV-2 vaccine candidates. Signal Transduct Target Ther 5(1):237. https://doi.org/10.1038/s41392-020-00352-y

2. Bedford J, Enria D, Giesecke J, Heymann DL, Ihekweazu C, Kobinger G, Lane HC, Memish Z, Oh MD, Schuchat A, Ungchusak K, Wieler LH (2020) COVID-19: towards controlling of a pandemic. The Lancet 395(10229):1015–1018. https://doi.org/10.1016/s0140-6736(20)30673-5

3. Panpradist N, Wang Q, Ruth PS, Kotnik JH, Oreskovic AK, Miller A, Stewart SW, Vrana J, Han PD, Beck IA, Starita LM, Frenkel LM, Lutz BR (2021) Simpler and faster Covid-19 testing: strategies to streamline SARS-CoV-2 molecular assays. EBioMedicine 64:103236. https://doi.org/10.1016/j.ebiom.2021.103236

4. Osmanodja B, Budde K, Zickler D, Naik MG, Hofmann J, Gertler M, Hülso C, Rössig H, Horn P, Seybold J, Lunow S, Bothmann M, Barrera-Pesek A, Mayrdorfer M (2021) Accuracy of a novel SARS-CoV-2 antigen-detecting rapid diagnostic test from standardized self-collected anterior nasal swabs. J Clin Med 10(10). https://doi.org/10.3390/jcm10102099

5. Kucirka LM, Lauer SA, Laeyendecker O, Boon D, Lessler J (2020) Variation in false-negative rate of reverse transcriptase polymerase chain reaction-based SARS-CoV-2 tests by time since exposure. Ann Intern Med 173(4):262–267. https://doi.org/10.7326/M20-1495

6. Zhang Z, Wang X, Wei X, Zheng SW, Lenhart BJ, Xu P, Li J, Pan J, Albrecht H, Liu C (2021) Multiplex quantitative detection of SARS-CoV-2 specific IgG and IgM antibodies based on DNA-assisted nanopore sensing. Biosens Bioelectron 181:113134. https://doi.org/10.1016/j.bios.2021.113134

7. Liu H, Dai E, Xiao R, Zhou Z, Zhang M, Bai Z, Shao Y, Qi K, Tu J, Wang C, Wang S (2021) Development of a SERS-based lateral flow immunoassay for rapid and ultra-sensitive detection of anti-SARS-CoV-2 IgM/IgG in clinical samples, Sens Actuators B Chem 329:129196. https://doi.org/10.1016/j.snb.2020.129196

8. Wang A, You X, Liu H, Zhou J, Chen Y, Zhang C, Ma K, Liu Y, Ding P, Qi Y, Zhang G (2022) Development of a label free electrochemical sensor based on a sensitive monoclonal antibody for the detection of tiamulin. Food Chem 366:130573. https://doi.org/10.1016/j.foodchem.2021.130573

9. Eissa S, Zourob M (2021) Development of a low-cost cotton-tipped electrochemical immunosensor for the detection of SARS-CoV-2. Anal Chem 93(3):1826–1833. https://doi.org/10.1021/acs.analchem.0c04719

10. Aydın EB, Aydın M, Sezgintürk MK (2021) Highly selective and sensitive sandwich immunosensor platform modified with MUA-capped GNPs for detection of spike Receptor Binding Domain protein: a precious marker of COVID 19 infection. Sens Actuators B Chem 345:130355. https://doi.org/10.1016/j.snb.2021.130355

11. V'kovski P, Kratzel A, Steiner S, Stalder H, Thiel V (2021) Coronavirus biology and replication: implications for SARS-CoV-2. Nat Rev Microbiol 19(3):155–170. https://doi.org/10.1038/s41579-020-00468-6

12. Paludan SR, Mogensen TH (2022) Innate immunological pathways in COVID-19 pathogenesis. Sci Immunol 7(67). https://doi.org/10.1126/sciimmunol.abm5505

13. Komiyama M (2022) Molecular mechanisms of the medicines for COVID-19. Bullet Chem Soc Japan 95(9):1308–1317. https://doi.org/10.1246/bcsj.20220179

14. Komiyama M (2021) Molecular-level anatomy of SARS-CoV-2 for the battle against the COVID-19 pandemic. Bullet Chem Soc Japan 94(5):1478–1490. https://doi.org/10.1246/bcsj.20210030

15. Lan J, Ge J, Yu J, Shan S, Zhou H, Fan S, Zhang Q, Shi X, Wang Q, Zhang L, Wang X (2020) Structure of the SARS-CoV-2 spike receptor-binding domain bound to the ACE2 receptor. Nature 581(7807):215–220. https://doi.org/10.1038/s41586-020-2180-5

16. van Eijk LE, Binkhorst M, Bourgonje AR, Offringa AK, Mulder DJ, Bos EM, Kolundzic N, Abdulle AE, van der Voort PH, Olde Rikkert MG, van der Hoeven JG, den Dunnen WF, Hillebrands JL, van Goor H (2021) COVID-19: immunopathology, pathophysiological mechanisms, and treatment options. J Pathol 254(4):307–331. https://doi.org/10.1002/path.5642

17. Cho IH, Kim DH, Park S (2020) Electrochemical biosensors: perspective on functional nanomaterials for on-site analysis. Biomater Res 24:6. https://doi.org/10.1186/s40824-019-0181-y

18. Yu S, Cao X, Yu M (2012) Electrochemical immunoassay based on gold nanoparticles and reduced graphene oxide functionalized carbon ionic liquid electrode. Microchem J 103:125–130. https://doi.org/10.1016/j.microc.2012.02.002

19. Sha Y, Guo Z, Chen B, Wang S, Ge G, Qiu B, Jiang X (2015) A one-step electrochemiluminescence immunosensor preparation for ultrasensitive detection of carbohydrate antigen 19–9 based on multi-functionalized graphene oxide. Biosens Bioelectron 66:468–73. https://doi.org/10.1016/j.bios.2014.12.013

20. Shen J, Shi M, Li N, Yan B, Ma H, Hu Y, Ye M (2010) Facile synthesis and application of Ag-chemically converted graphene nanocomposite. Nano Res 3(5):339–349. https://doi.org/10.1007/s12274-010-1037-x

21. Huang X, Deng X, Zhu H, Qi W, Wu D (2018) Ag@Fe2O3-graphene oxide nanocomposite as a novel redox probe for electrochemical immunosensor for alpha-fetoprotein detection. J Solid State Electrochem 23(2):335–343. https://doi.org/10.1007/s10008-018-4139-0

22. Han L, Liu CM, Dong SL, Du CX, Zhang XY, Li LH, Wei Y (2017) Enhanced conductivity of rGO/Ag NPs composites for electrochemical immunoassay of prostate-specific antigen. Biosens Bioelectron 87:466–472. https://doi.org/10.1016/j.bios.2016.08.004

23. Salgado S, Pu L, Maheshwari V (2012) Targeting chemical morphology of graphene oxide for self-assembly and subsequent templating of nanoparticles: a composite approaching capacitance limits in grapheme. J Phys Chem C 116(22):12124–12130. https://doi.org/10.1021/jp3023875

24. Xiao H, Wei S, Gu M, Chen Z, Cao L (2021) A sandwich-type electrochemical immunosensor using rGO-TEPA-Thi-Au as sensitive platform and CMK-3@AuPtNPs as signal probe for AFP detection. Microchem J 170. https://doi.org/10.1016/j.microc.2021.106641

25. Yan Q, Cao L, Dong H, Tan Z, Hu Y, Liu Q, Liu H, Zhao P, Chen L, Liu Y, Li Y, Dong Y (2019) Label-free immunosensors based on a novel multi-amplification signal strategy of TiO2-NGO/Au@Pd hetero-nanostructures. Biosens Bioelectron 127:174–180. https://doi.org/10.1016/j.bios.2018.12.038

26. Li J, Jin H, Wei M, Ren W, Wang J, Zhang Y, Wu L, He B (2021) Dual mode competitive electrochemical immunoassay for dibutyl phthalate detection based on PEI functionalized nitrogen doped graphene-CoSe2/gold nanowires and thionine-Au@Pt core-shell. Sens Actuators B Chem 331. https://doi.org/10.1016/j.snb.2020.129401

27. Chen J, Yu C, Zhao Y, Niu Y, Zhang L, Yu Y, Wu J, He J (2017) A novel non-invasive detection method for the FGFR3 gene mutation in maternal plasma for a fetal achondroplasia diagnosis based on signal amplification by hemin-MOFs/PtNPs. Biosens Bioelectron 91:892–899. https://doi.org/10.1016/j.bios.2016.10.067

28. Lakshmipriya T, Gopinath SC, Tang TH (2016) Biotin-streptavidin competition mediates sensitive detection of biomolecules in enzyme linked immunosorbent assay. PLoS One 11(3):e0151153. https://doi.org/10.1371/journal.pone.0151153

29. Wang Y, Zhao G, Wang H, Zhang Y, Zhang N, Wei D, Feng R, Wei Q (2020) Label-free electrochemical immunosensor based on biocompatible nanoporous Fe3O4 and biotin-streptavidin system for sensitive detection of zearalenone, Analyst 145(4):1368–1375. https://doi.org/10.1039/c9an02543j

30. Ji R, Chen S, Xu W, Qin Z, Qiu JF, Li CR (2018) A voltammetric immunosensor for clenbuterol based on the use of a MoS2-AuPt nanocomposite. Mikrochim Acta 185(4):209. https://doi.org/10.1007/s00604-018-2746-1

31. Gurunathan S, Han JW, Dayem AA, Eppakayala V, Kim JH (2012) Oxidative stress-mediated antibacterial activity of graphene oxide and reduced graphene oxide in Pseudomonas aeruginosa. Int J Nanomed 7:5901–14. https://doi.org/10.2147/IJN.S37397

32. Dikin DA, Stankovich S, Zimney EJ, Piner RD, Dommett GH, Evmenenko G, Nguyen ST, Ruoff RS (2007) Preparation and characterization of graphene oxide paper, Nature 448(7152):457–460. https://doi.org/10.1038/nature06016

33. Huang L, Wang Z, Zhang J, Pu J, Lin Y, Xu S, Shen L, Chen Q, Shi W (2014) Fully printed, rapid-response sensors based on chemically modified graphene for detecting NO2 at room temperature. ACS Appl Mater Interfaces 6(10):7426–33. https://doi.org/10.1021/am500843p

34. McAllister MJ, Li JL, Adamson DH, Schniepp HC, Abdala AA, Liu J, Herrera-Alonso M, Milius DL, Car R, Prud'homme RK, Aksay IA (2007) Single sheet functionalized graphene by oxidation and thermal expansion of graphite. Chem Mater 19(18):4396–4404. https://doi.org/10.1021/cm0630800

35. Das TR, Sharma PK (2020) Hydrothermal-assisted green synthesis of Ni/Ag@rGO nanocomposite using Punica granatum juice and electrochemical detection of ascorbic acid. Microchem J 156. https://doi.org/10.1016/j.microc.2020.104850

36. Hou L, Huang Y, Hou W, Yan Y, Liu J, Xia N (2020) Modification-free amperometric biosensor for the detection of wild-type p53 protein based on the in situ formation of silver nanoparticle networks for signal amplification. Int J Biol Macromol 158:580–586. https://doi.org/10.1016/j.ijbiomac.2020.04.271

37. Lee SJ, Anandan V, Zhang G (2008) Electrochemical fabrication and evaluation of highly sensitive nanorod-modified electrodes for a biotin/avidin system. Biosens Bioelectron 23(7):1117–24. https://doi.org/10.1016/j.bios.2007.10.025

38. Yin Z, Wu J, Yang Z (2011) Amperometric sensors based on Ni/Al and Co/Al layered double hydroxides modified electrode and their application for hydrogen peroxide detection. Biosens Bioelectron 26(5):1970–4. https://doi.org/10.1016/j.bios.2010.08.049

39. Wang P, Pei F, Ma E, Yang Q, Yu H, Liu J, Li Y, Liu Q, Dong Y, Zhu H (2020) The preparation of hollow AgPt@Pt core-shell nanoparticles loaded on polypyrrole nanosheet modified electrode and its application in immunosensor. Bioelectrochemistry 131:107352. https://doi.org/10.1016/j.bioelechem.2019.107352

40. Winefordner JD, Long GL (1983) Limit of detection. Anal Chem 55(7):712A-724A. https://doi.org/10.1021/ac00258a001

41. Vadlamani BS, Uppal T, Verma SC, Misra M (2020) Functionalized TiO2 nanotube-based electrochemical biosensor for rapid detection of SARS-CoV-2. Sensors (Basel) 20(20). https://doi.org/10.3390/s20205871

42. Mojsoska B, Larsen S, Olsen DA, Madsen JS, Brandslund I, Alatraktchi FA (2021) Rapid SARS-CoV-2 detection using electrochemical ummunosensor. Sensors (Basel) 21(2). https://doi.org/10.3390/s21020390

43. Yang Y, Zhao R, Wang Y, Song D, Jiang B, Guo X, Liu W, Long F, Song H, Hao R (2022) Rapid and universal detection of SARS-CoV-2 and influenza A virus using a reusable dual-channel optic fiber immunosensor. J Med Virol 94(11):5325–5335. https://doi.org/10.1002/jmv.28015

44. Erdem A, Senturk H, Yildiz E, Maral M (2022) Amperometric immunosensor developed for sensitive detection of SARS-CoV-2 spike S1 protein in combined with portable device. Talanta 244:123422. https://doi.org/10.1016/j.talanta.2022.123422